

## الروتاري بالموجات فوق الصوتية بالقطع من لومينا السيراميك: دراسة تجريبية والاستفادة المثلى من ردود الآلات

رافي براتاب سينغ\*،\*\* وسانديب سينغال\*،#

\* قسم الهندسة الميكانيكية، المعهد الوطني للتكنولوجيا، كوروكشتر، هاريانا، الهند

\*\* المراسلة على البريد الإلكتروني: #ravipratap.1512@gmail.com sandeep—singhal—reck@rediffmail.com

### الخلاصة

في الهيكل التنافسي الحالي للصناعات التحويلية والتطبيقات الصناعية، لوحظت اللومينا السيراميك بشكل جيد باعتبارها واحدة من السيراميك المتقدمة المطلوبة للغاية بسبب خصائص متفوقة ومتفوقة. والهدف من هذه المقالة هو التحقيق تجريبيا تأثير العديد من المتغيرات العملية وهي: سرعة المغزل، معدل التغذية، ضغط المبرد، والموجات فوق الصوتية السلطة على أداء الآلات المختلفة. خشونة السطح، وسمك التقطع. وقد استخدمت منهجية سطح الاستجابة لتصميم التجارب. وقد تم تقييم المجهرية من عينات تشكيله وتحليلها من خلال المجهر الإلكتروني الماسح الضوئي. وقد لوحظ وجود تشوه البلاستيك جنبا إلى جنب مع كسر هش يهيمن عليها بالقطع بالموجات فوق الصوتية من اللومينا السيراميك. وقد لوحظ أن معدل التغذية وسرعة المغزل باعتبارها المعلمات الأكثر تأثيرا التي تحكم وضع تشوه في لومينا السيراميك. تم أيضا تحسين استجابات الآلات باستخدام نظرية الرغبة، ووضع الحدود المثلى، وكانت القيم التجريبية التي تم الحصول عليها لخشونة السطح وسمك التقطع هما 0.134 ميكرو متر و 0.073 مم، على التوالي.

## Rotary ultrasonic machining of alumina ceramic: Experimental study and optimization of machining responses

Ravi Pratap Singh\*, \*\*\*, and Sandeep Singhal\*\*, #

\*Assistant Professor, Department of Industrial & Production Engineering, Dr. B. R. Ambedkar National Institute of Technology, Jalandhar, Punjab, India

\*\*Associate Professor, Department of Mechanical Engineering, National Institute of Technology, Kurukshetra, Haryana, India

\*\*\* Corresponding Author: ravipratap.1512@gmail.com; #sandeep\_singhal\_reck@rediffmail.com

### ABSTRACT

In the present competitive structure of manufacturing and industrial applications, alumina ceramic has been well observed as one of the highly demanded advanced ceramics owing to its excellent and superior properties. The objective of this article is to experimentally investigate the influence of several process variables, namely, spindle speed, feed rate, coolant pressure, and ultrasonic power on different machining performances, that is, surface roughness and chipping thickness. Response surface methodology has been employed to design the experiments. Microstructure of the machined samples has been evaluated and analyzed through scanning electron microscope. The existence of plastic deformation has also been observed along with the dominated brittle fracture in rotary ultrasonic machining of alumina ceramic. Feed rate and spindle speed have been observed as the most influential parameters that govern the deformation mode in alumina ceramic. The optimization of machining responses has also been conducted by employing desirability theory, and at an optimized parametric setting, the obtained experimental values for surface roughness and chipping thickness are 0.134  $\mu\text{m}$  and 0.073 mm, respectively.

**Keywords:** Rotary ultrasonic machining; alumina ceramic; surface roughness; chipping thickness; response surface methodology.

### ABBREVIATION

USM	Ultrasonic Machining
EDM	Electrical Discharge Machining
LBM	Laser Beam Machining
RUM	Rotary Ultrasonic Machining
MRR	Material Removal Rate
CFRP/Ti	Carbon Fiber Reinforced Polymer/Titanium
CS	Chipping Size
SR	Surface Roughness
CT	Chipping Thickness
CCRD	Central Composite Rotatable Design
SEM	Scanning Electron Microscopy
EDX	Energy Dispersive X-ray

## NOMENCLATURE

dof	Degree of Freedom
F	Fisher's ratio
Do	Outer diameter of tool
Di	Inner diameter of tool
R2	Coefficient of determination
$\sigma$	Stress distribution

## INTRODUCTION

In the family of advanced engineering ceramics, alumina ceramic ( $Al_2O_3$ ) is known as one of the most demanding materials, which possesses excellent and superior thermal, mechanical, and electrical properties. Owing to the above stated finer properties of alumina ceramic, it covers a wide range of applications in numerous industries such as aerospace, automobile, electronics, and cutting tools manufactures (Jiao et al., 2005; Li et al., 2006; Zeng et al., 2009). Despite of its excellent properties, its machining with conventional methods becomes quite tougher and causes high processing cost and lesser accuracy, which further hindered its expansion into the market (Liet al., 2006; Gonget al., 2010). In the literature, alumina ceramic has also been reported to be processed with advanced machining methods, that is, USM, EDM, LBM, and so on. However, the processing of alumina ceramic with these manufacturing methods does not provide fruitful solutions and casually results in several drawbacks such as heat affected zone, geometrical inaccuracies (conicity, out of roundness, etc.), recast layer formation, and lesser material removal rate (Li et al., 2006; Kataria et al., 2015; Dubey & Yadava, 2008; Patel et al., 2011; Singh & Singhal, 2016a). Hence, there is a decisive exigency to cultivate a prudent and highly accurate machining solution that can process this highly demanding ceramic precisely.

Among the available advanced machining methods introduced for processing typical and advanced materials (i.e., ceramics, composites, hard-to-machine materials, etc.), RUM method has been observed as one of the best suitable candidates that fits for precise processing of the alumina ceramic material as this process produces thermal damage free profiles along with high accuracy and enhanced material removal rate (Li et al., 2006; Gong et al., 2010; Singh & Singhal, 2016c).

RUM is a hybrid non-traditional machining solution that merges the mechanisms of conventional grinding and static USM, reporting with more enhance MRR than that attained by either static USM or diamond grinding, utilized potentially to machine a wide range of the latest and difficult-to-machine materials (Li et al., 2006; Singh & Singhal, 2016a; Geng et al., 2014). The mechanisms of material removal in RUM process have been found to be brittle fracture or micro level chipping of the work surface. However, the removal of material can also take place by plastic deformation under the condition of very lower feed rate with high spindle speed (Singh & Singhal, 2016d; Pei et al., 1995). RUM is also considered as non-chemical, non-thermal, and non-electrical machining method (Gong et al., 2010; Singh & Singhal, 2016b; Kataria et al., 2016b).

## LITERATURE REVIEW

Cong et al. (2014) carried out an experimental investigation with a view to appraise the efficacy of several process factors on quality attributes in RUM of CFRP/Ti stacks. Spindle rotational speed was not found to be significant for MRR while machining the CFRP composites with RUM, whereas MRR increases linearly as the feed rate increases (Cong et al., 2012). Li et al. (2005) experimentally studied the process variables. When SiC matrix composites were machined with RUM internal flanging and voids on the tool face were found to be influential for MRR directly, and MRR of 13.0mm<sup>3</sup>/s was obtained (Bertsche et al., 2013). In RUM of glass, it was found that higher MRR was attained with RUM than that produced with the stationary USM process (Ya et al., 2001). For RUM of titanium alloy, MRR increased as the feed rate increased, whereas the ultrasonic power and spindle speed had no significant effect on MRR. Hu et al. (2002) utilized the design of experiments to read out the impact of input factors on MRR.

An experimental study on optical K9 glass (Singh & Singhal, 2016b; Zhang et al., 2014) shows the feed rate as the most influential factor that affects CS compared to other parameters such as ultrasonic power and spindle speed. It was also stated that the consequence of a lower level of feed rate on the size of chipping was stronger than higher spindle speed (Zhang et al., 2011; Singh & Singhal, 2016c). In RUM of macor dental ceramics (Churi et al., 2009), the results showed that spindle speed at a higher level, feed rate at a lower level, and ultrasonic power at lower level resulted in reduced chipping size. Liu et al. (2014) optimized the parametric setting for chipping minimization while performing RUM of alumina oxide ceramic using diamond drills, and the optimized setting value of exit crack was 25.378  $\mu\text{m}$ .

## SCOPE OF THE PRESENT RESEARCH

It is revealed from the literature review that there are almost some few research studies that have been conducted on RUM of alumina ceramic employing the response surface methodology (RSM) with a view to scheme the experiments and also to assess parameters' influences on process responses. The parameter termed "coolant pressure" has been omitted throughout all the investigation performed in RUM of alumina ceramic. Ultrasonic power has also been investigated at a very low level (30-40%) in past research studies. There is a need to expose the machining of alumina ceramic at higher power levels. Optimization of machining characteristics, that is, SR (Ra) and CT, has also never been attempted earlier in RUM of alumina ceramic. The optimization of the machining responses will further make the process applicability more meaningful while tackling real life industrial problems (Kataria et al., 2016a; Singh et al., 2015; Singh & Singhal, 2016d).

In light of the above discussion, the present article has been targeted to explore the impact of several process factors such as feed rate, spindle speed, ultrasonic power, and coolant pressure on SR (Ra) and CT in RUM of alumina ceramic by using RSM in the form of CCRD. The mathematical model developed through this approach will be helpful in industrial revelation. SEM analysis of machined samples has been presented. Optimization has also been attempted for SR (Ra) and CT, using desirability approach.

## MATERIALS AND METHODS

The fabrication work of alumina ceramic ( $\text{Al}_2\text{O}_3$ ) material was carried out at Ants Ceramics Pvt. Ltd. (Thane, India). The process of alumina ceramic material fabrication includes a shaping process called “slip casting” followed by a sintering operation performed for the desired compaction and denseness of ceramic. The manufacturing process of alumina ceramic consists of several steps and is demonstrated in Figure 1. To produce alumina ceramic material, alpha phase alumina, having a mean particle size of 2-4  $\mu\text{m}$ , was utilized as base material. After the perfect blending of raw material, slips have been prepared, and then these slips are poured into the mould of the desired shape (rectangular shaped). The slip casted product (green compact) was further allowed for drying in oven 70 °C for approximately one hour and successively placed into an electric furnace for the purpose of sintering (Falamaki & Beyhaghi, 2009).

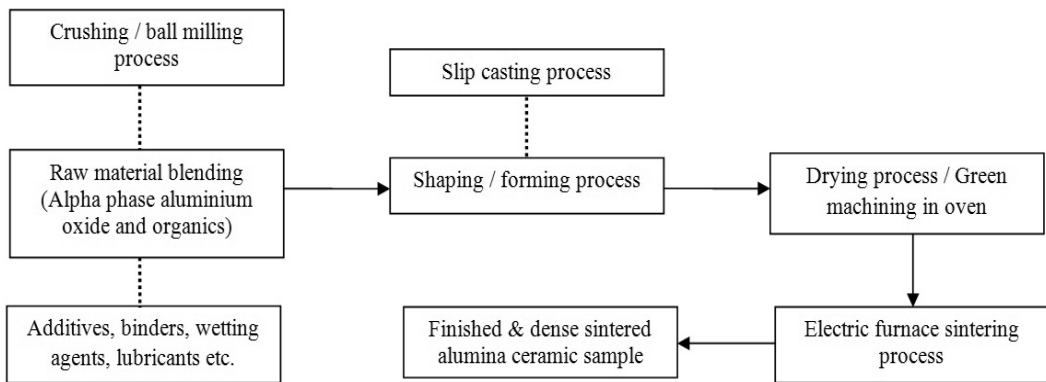


**Figure 1.** Procedure adopted for the fabrication of alumina ceramic material.

The fabricated alumina ceramic material is characterized using EDX test and SEM. The SEM microstructure of the alumina ceramic workpiece at 1000 $\times$  and 3000 $\times$ , before machining, is depicted in Figure 2. This reveals the majorly uniformly distributed aluminium oxide compound throughout the surface. It has also been observed from EDX analysis that the majority of portion is covered with aluminium oxide compound, as shown in Figure 3.

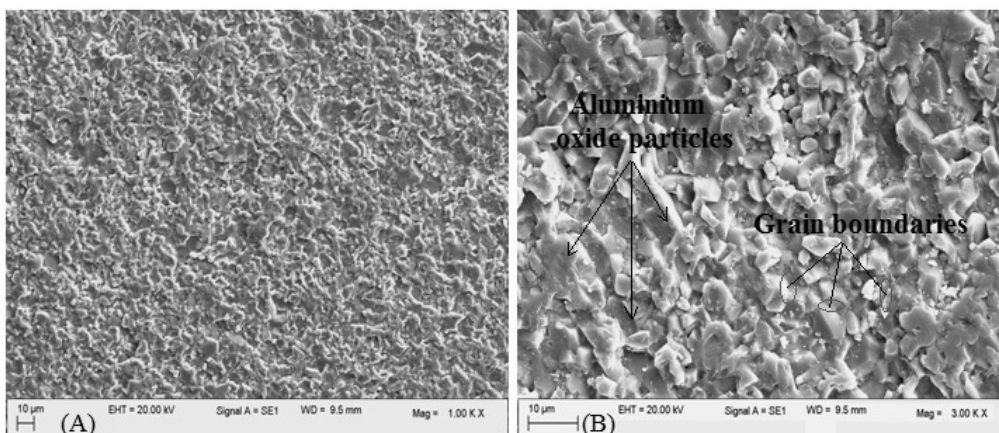


**Figure 2.** SEM microstructure of alumina ceramic surface before machining at (A) 1000 $\times$  and (B) 3000 $\times$ .

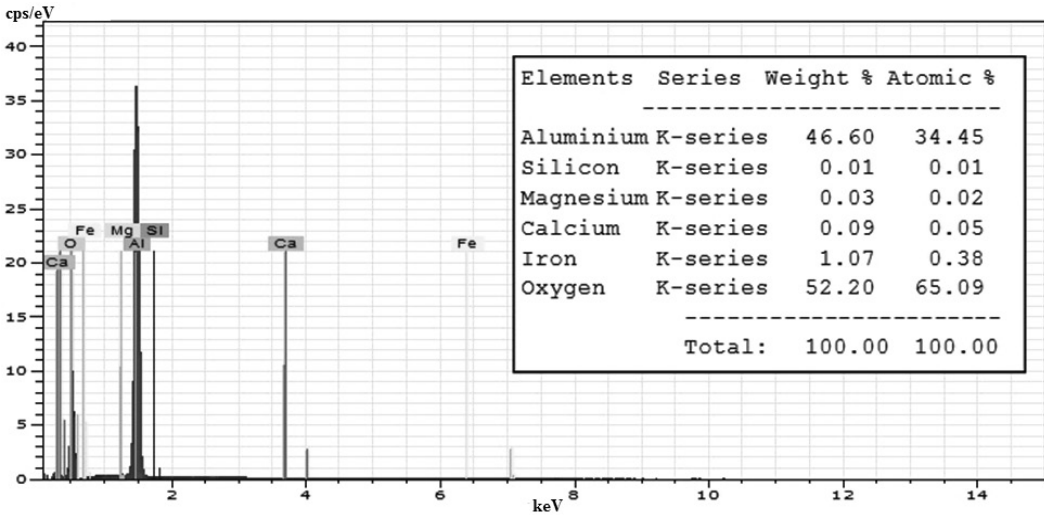


Figure 3. EDX analysis of alumina ceramic.

The present investigation involves the rotary ultrasonic drilling of alumina ceramic under the influence of a distinctive set of experimental conditions. Tables 1 and 2 are demonstrating the chemical composition and several work material properties, respectively.

Table 1. Chemical compositions of alumina ceramic.

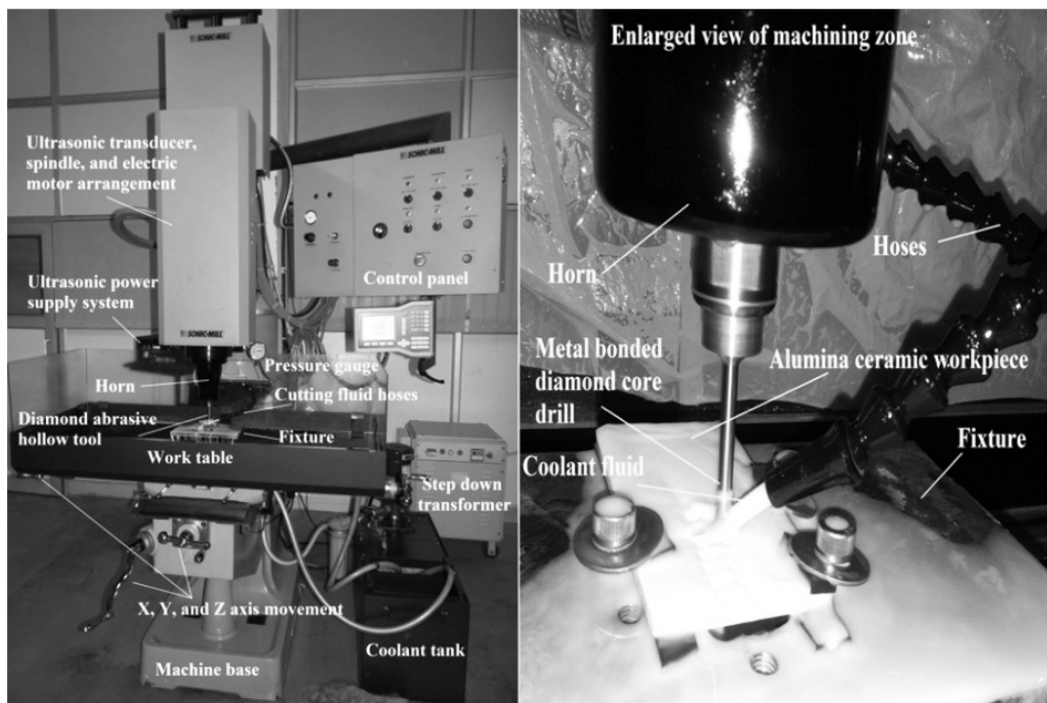
Chemical compound composition (vol. %)						
Al <sub>2</sub> O <sub>3</sub>	SiO <sub>2</sub>	MgO	Na <sub>2</sub> O	Fe <sub>2</sub> O <sub>3</sub>	CaO	
99.7	0.05	0.08	0.03	0.015	0.03	

Table 2. Mechanical properties of alumina ceramic (Al<sub>2</sub>O<sub>3</sub>).

Parameters	Unit of measures	Values
Density	gm/cm <sup>3</sup>	3.85
Flexural strength	MPa	379
Elastic modulus	GPa	375
Shear modulus	GPa	152
Bulk modulus	GPa	228
Compressive strength	MPa	2600
Tensile strength	MPa	275
Hardness	VHN	18.3
Thermal conductivity	W/m <sup>o</sup> K	35
Fracture toughness	MPa√m	4.0
Coefficient of thermal expansion	×10 <sup>6</sup> /°C	8.4

To investigate SR and CT in RUM of alumina ceramic material, feed rate, spindle speed, ultrasonic power, and coolant pressure were selected as input factors. The different sets of experimental conditions were attained by varying the selected parameters in their defined range, while other machining conditions or parameters were kept unchanged throughout the experimentation work as represented in Table 3. The pilot experimentation has been conducted by varying a single factor at a time, whereas other variables were kept fixed at baseline. Experimental trials were performed with a view to select the levels and range of the considered process variables by observing the trends of impact of these variables on the considered responses of interest. The fixture was fabricated for placing the workpiece under the cutting tool.

In the present work, alumina ceramic (99.7%  $\text{Al}_2\text{O}_3$ ) has been selected as work material with the dimensions of  $105 \times 55 \times 4$  mm. Metal bonded (bond type: B) diamond impregnated core drill was utilized for conducting the experimentation work. The inner and outer diameters of the hollow tool were 4 mm and 5 mm, correspondingly. The diamond abrasive grits bonded over the tool tip were having a mesh size of 220. The core drill was having the tuning length of 58 mm. Blascut BC 20 SW water miscible serous (Blaser Swisslube Inc., NY, USA) was utilized as the coolant after being diluted with deionized water at 1-18 ratio.



**Figure 4.** Detailed illustration of rotary ultrasonic machine set-up.

The experimentation was performed on “Series10 Knee-mill” rotary ultrasonic machine set-up (Sonic Mill, Albuquerque, NM, USA). Figure 4 illustrates the major constituents of RUM set-up along with its machining zone. The machining zone consisting of horn, fixture, diamond core drill, alumina ceramic workpiece, and coolant fluid flow is also represented in Figure 4.

## EXPERIMENTAL PROCEDURE

In the current study, the main experiments were planned and designed by using a design of experiments technique called “response surface methodology (RSM)” through CCRD. For this purpose, a statistical software known as “Design Expert 9.0” (State-Ease, Inc., USA) was utilized. There were a total of four process variables in the experimental plan, and all were having five levels. As per the experimental design plan, all the 30 runs were conducted in a complete randomized manner with a view to minimize the experimental error. As per the designed experimental matrix, holes were drilled in the alumina ceramic workpiece under different operating conditions. The entire experimental plan was replicated twice, that is, consisting of total 60 runs. For further statistical analysis, a mean value of two observations is considered. Table 4 represents the complete experimental design plan along with the average values of SR and CT. In the present work, both SR and CT were explored to evaluate the quality of drilled hole in RUM of alumina ceramic. The CT on the machined rod was inspected by employing an optical microscope (Olympus America Inc., NY, USA), and the quantification of CT was made by utilizing a digital vernier caliper (Mitutoyo Corp., Japan).

**Table 3.** Considered process variables with their levels.

Symbols	Parameters	Level 1	Level 2	Level 3	Level 4	Level 5
A	Feed rate (mm/sec)	0.012	0.024	0.036	0.048	0.060
B	Spindle speed (rpm)	2500	3000	3500	4000	4500
C	Ultrasonic power (%)	20	30	40	50	60
D	Coolant pressure (kPa)	140	175	210	245	280

### *Constant parameters / experimental conditions*

Coolant fluid used	Blasocut BC 20 SW	Abrasive concentration (%)	100
Vibration frequency	20.43±0.05 kHz	Diamond abrasive grit size	220 mesh
Tool bond type	B type (metal bonded)	Tool type	Non-slotted
Coolant to water ratio	1:18 (by volume)	Compressed air pressure	560 kPa

**Table 4.** CCRD based design matrix and results.

Exp. No.	Process parameters	Characteristics				
		Feed rate (mm/s)	Spindle speed (rpm)	Ultrasonic power (%)	Coolant pressure (kPa)	Ra ( $\mu\text{m}$ )
1.	0.024	3000	30	175	0.609	0.488
2.	0.048	3000	30	175	0.838	0.879
3.	0.024	4000	30	175	0.532	0.390
4.	0.048	4000	30	175	0.949	0.680
5.	0.024	3000	50	175	0.592	0.396
6.	0.048	3000	50	175	0.899	0.815
7.	0.024	4000	50	175	0.389	0.308
8.	0.048	4000	50	175	0.931	0.553
9.	0.024	3000	30	245	0.589	0.510
10.	0.048	3000	30	245	0.859	0.750
11.	0.024	4000	30	245	0.402	0.450
12.	0.048	4000	30	245	0.895	0.596
13.	0.024	3000	50	245	0.489	0.440
14.	0.048	3000	50	245	0.873	0.789
15.	0.024	4000	50	245	0.352	0.272
16.	0.048	4000	50	245	0.831	0.482
17.	0.012	3500	40	210	0.289	0.192
18.	0.060	3500	40	210	1.241	0.972
19.	0.036	2500	40	210	0.759	0.810
20.	0.036	4500	40	210	0.665	0.526
21.	0.036	3500	20	210	0.820	0.670
22.	0.036	3500	60	210	0.718	0.583
23.	0.036	3500	40	140	0.859	0.520
24.	0.036	3500	40	280	0.761	0.462
25.	0.036	3500	40	210	0.749	0.840
26.	0.036	3500	40	210	0.869	0.790
27.	0.036	3500	40	210	0.899	0.851
28.	0.036	3500	40	210	0.867	0.748
29.	0.036	3500	40	210	0.839	0.920
30.	0.036	3500	40	210	0.879	0.810

RSM approach is used for the purpose of modeling and analyzing the problem under consideration. Box and Wilson in 1951 have given this method to develop the relationship between process variables and considered responses in an effective manner (Singh et al., 2014). The interpretation of the system's behavior can be made through a developed regression model. A general second order polynomial quadratic model is expressed as follows:

$$Z = \alpha_0 + \sum_{j=1}^p \alpha_j Y_j + \sum_{j=1}^p \alpha_{jj} Y_j^2 + \sum_{j<m}^p \alpha_{jm} Y_j Y_m + \dots \quad (1)$$

where 'Z' is the considered process responses, 'Y<sub>j</sub>' (1,2,3,...,p) is the independent of 'p' quantitative input factors, and  $\alpha_0$ ,  $\alpha_j$ ,  $\alpha_{jj}$ , and  $\alpha_{jm}$  are the regression coefficients. The 2<sup>nd</sup>, 3<sup>rd</sup>, and 4<sup>th</sup> terms of the quadratic equation represent the linear effects, higher order effects, and interactive effects, respectively. For the present study, this equation can be expressed by using the terms Y<sub>1</sub>, Y<sub>2</sub>, Y<sub>3</sub>, and Y<sub>4</sub> to represent feed rate, spindle speed, ultrasonic power, and coolant pressure, respectively.

$$Z = \alpha_0 + \alpha_1 Y_1 + \alpha_2 Y_2 + \alpha_3 Y_3 + \alpha_4 Y_4 + \alpha_{11} Y_1^2 + \alpha_{22} Y_2^2 + \alpha_{33} Y_3^2 + \alpha_{44} Y_4^2 + \alpha_{12} Y_1 Y_2 + \alpha_{13} Y_1 Y_3 + \alpha_{14} Y_1 Y_4 + \alpha_{23} Y_2 Y_3 + \alpha_{24} Y_2 Y_4 + \alpha_{34} Y_3 Y_4 \quad (2)$$

## RESULTS AND DISCUSSION

The experimental results for investigated process characteristics, that is, SR and CT, are exemplified in Table 4. The variance analysis (ANOVA) test was also performed with a view to examine the significance of the developed models. The ANOVA test results for the considered process responses are detailed in Tables 5 (for SR (Ra)) and 6 (for CT), respectively.

### *Adequacy check of ANOVA model for SR (Ra) and CT*

On the basis of the ANOVA test outcomes detailed in Tables 5 and 6, the values of the probability term "Prob>F" (<0.0500) statistically confirm the significance of model terms at 95% confidence interval level. The models with F-values of 37.59 and 39.02 entail that both models are statistically considerable and fit the data more satisfactorily. For both models, "p-value" is 0.3866 (SR (Ra)) and 0.6336 (CT) for the term "lack of fit," which confirms its irrelevance in context to the pure error. This also makes sure that the developed polynomial regression model is well fitting the entire scheme points. The percent contribution of "pure error" for SR and CT is 1.08% and 1.36%, respectively. This quite smaller magnitude of pure error for both models reveals that there is nearly negligible deviation in the experimental results caused by error and therefore, in the current study, the deviation through the investigated process variables outweighs the variation through error. This further makes the ANOVA analysis and its results lawful. 'R<sup>2</sup>' (called "coefficient of determination") is another imperative coefficient in the ANOVA analysis, which explicates the model variability in percentage concerning the actual data variability in totality. The developed model entails the best elucidation of experimental data if the value of 'R<sup>2</sup>' term approaches unity. The computed values of 0.9442 and 0.9536 in Tables 5 and 6, correspondingly, signify that the model explicates 94.42% and 95.36% variability of SR and CT, respectively. To confirm whether

the model has described the well relationship between process variables and process responses, the ‘predicted R<sup>2</sup>’ and ‘adjusted R<sup>2</sup>’ have been examined. For SR and CT, the values of the predicted R<sup>2</sup> (0.8205 and 0.8563) demonstrate a rational concurrence with the adjusted R<sup>2</sup> (0.9191 and 0.9291), respectively. The signal-to-noise ratio (S/N ratio) is exemplified through the term ‘adequate precision.’ The model will be fit to proceed further if the value of ‘adequate precision’ is greater than 4. The ratios of 24.042 and 20.195 designate satisfactory indications for the developed SR and CT models, respectively. The standard deviation to mean ratio is acknowledged as “coefficient of variation (CV),” which elucidates the relative variation. For SR and CT, the values of “coefficient of variation” are 8.14% and 8.98%, respectively, which further specify admirable accuracy and reliability of the experimentation conducted. Based on RSM approach, the developed models for SR and CT are represented in Eqns. (3) and (4), after employing the method of “backward elimination” for obliterating “not significant” variables.

**Model for ‘SR (Ra)’ in terms of actual factors:**

$$SR (Ra) = -2.3103 + 7.3229 \times A + 0.0009844 \times B + 0.006957 \times D + 0.007718 \times A*B - 234.5920 \times A^2 - 0.0000001881 \times B^2 - 0.0003278 \times C^2 \tag{3}$$

**Model for ‘CT’ in terms of actual factors:**

$$CT = -7.0696 + 78.4430 \times A + 0.001337 \times B + 0.04201 \times C - 0.0052979 \times A*B - 472.9022 \times A^2 - 0.00000018649 \times B^2 - 0.00056997 \times C^2 - 0.000074182 \times D^2 \tag{4}$$

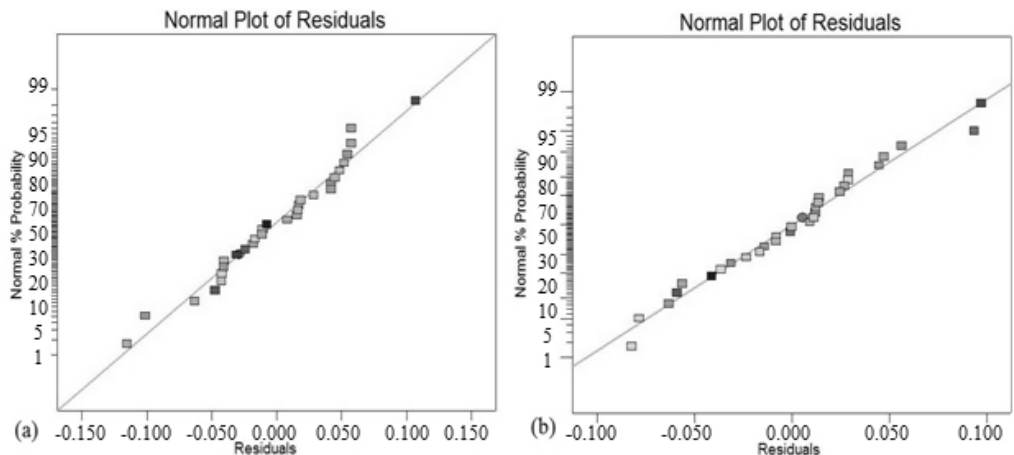


**Figure 5.** Residual plots of normal probability for (a) SR (Ra) and (b) CT

The normal probability plots of residuals for surface roughness (SR) and chipping thickness (CT), respectively, are illustrated in Figures 5(a) and 5(b). These plots reveal that most of the residuals are scattered out along the best fitted line, which further confirms the normally dispersing of the errors. Validation of the developed models is made by analyzing actual values with predicted values. Figures 6(a) and 6(b) show the actual values versus predicted values plots for SR and CT, respectively. As construed from these plots, the developed regression models are satisfactorily

attuned with the actual values. Therefore, the prediction made with the developed second order regression models for considered responses is validated with accuracy and dependability.

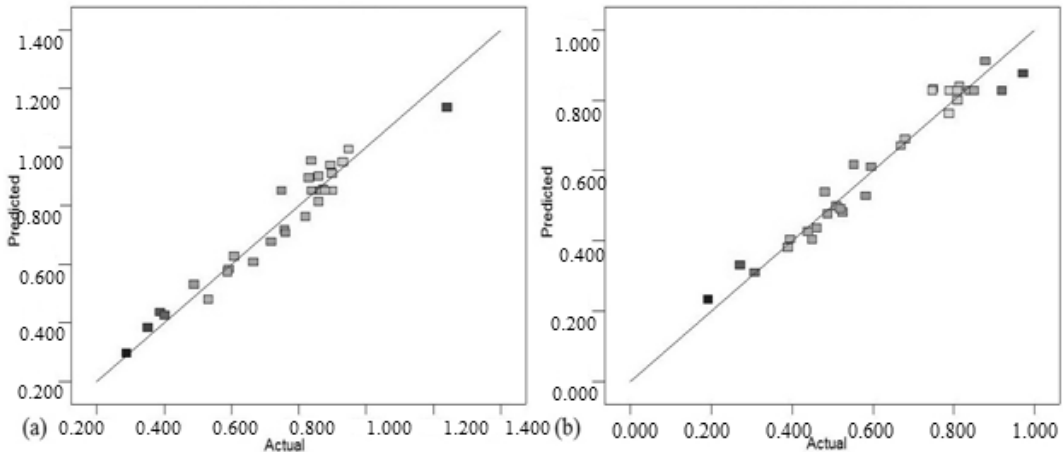


Figure 6. Predicted v/s actual plots for (a) SR (Ra) and (b) CT.

### *Influences of investigated process variables on 'SR (Ra)'*

In the RUM of alumina ceramic, the variables feed rate (A), spindle speed (B), coolant pressure (D), interactive impacts of feed rate and spindle speed ( $A \times B$ ), second order term of feed rate ( $A^2$ ), spindle speed ( $B^2$ ), and ultrasonic power ( $C^2$ ) are found to possess significant effects on the SR. The parameters, namely, feed rate (A) and coolant pressure (D) are observed to contribute approximately 82% of the overall disparity in the response data. All these linear, interaction effects and second order terms of input process parameters possessing main contribution for SR are well detailed in Table 5.

SR is found to increase steeply as the feed rate incremented from 0.012 mm/sec. to 0.060 mm/sec. However, the increment in spindle speed, coolant pressure, and ultrasonic power is reported with a gradual decrease in SR. The reported enhancement rate in SR with feed rate is higher than the decrement rate in SR with other parameters, as shown in the perturbation plot for SR in Figure 7.

Figure 8 depicts two factors interactive effect plots while processing alumina ceramic material ( $Al_2O_3$ ) with the RUM process. The combined influence of feed rate and spindle speed on SR is represented in Figure 8 (a). Higher SR is revealed as the feed rate of diamond impregnated core drill tool increases. The increment in the feed rate causes the increased indentation depth of the diamond abrasives, which further promotes the rough cutting of work surface (removal of material, through brittle fracture or in the form of bigger chunks); hence increased SR has been observed. The SR is found to be reduced at higher levels of spindle speed. As the spindle speed is enhanced from 2500 rpm to 4500 rpm, the chances of material to be removed in ductile mode are also enhanced, which further produces the finer machined surfaces. Furthermore, increased indentation length of abrasives (as spindle speed is enhanced) also makes the flow of coolant into the cutting region quite tough and hence the cooling effect gets reduced. This could cause a rise in

the local temperature of the machining region and, moreover, make the surface of work softer and reduce the propensity for brittle mode failure; thus reduced SR is observed. Figure 8(b) illustrates the combined effects of ultrasonic power and spindle speed on SR. The SR is observed to fall as the spindle speed level improved from 2500 rpm to 4500 rpm, whereas moderate decrement in SR is attained as the ultrasonic power incremented from 20 % to 60 %. The amplitude of vibration increases with ultrasonic power, which further promotes more effectual removal of swarf and debris through the appropriate flow of coolant fluid from the cutting region, hence resulting in a reduced level of surface roughness (from 0.820  $\mu\text{m}$  to 0.718  $\mu\text{m}$ ). Similar findings have been reported in different investigations carried out on RUM of ceramic materials. The combined influence of feed rate and coolant pressure on SR is described in Figure 8(c). An increment in SR with feed rate is observed to be more steep, whereas SR decreases gradually as the coolant pressure is improved. As the coolant pressure increases from 140 kPa to 280 kPa, SR also decrements from 0.859  $\mu\text{m}$  to 0.761  $\mu\text{m}$ . *The higher the coolant fluid pressure is, the faster the removal of debris and swarf from the machining zone will be.* This consequence further promotes the possibilities of getting better surface finish of the machined surface. The interaction between feed rate and spindle speed is also found to produce an appreciable effect on the surface roughness.

Table 5. ANOVA results for surface roughness (Ra)

Source	Sum of squares	dof	Mean square	F-value	p-value Prob> F	% Contribution
Model	1.23	9	0.14	37.59	< 0.0001*	
A-Feed Rate	1.05	1	1.05	289.02	< 0.0001*	80.76
B-Spindle Speed	0.018	1	0.018	4.91	0.0385*	1.38
C-Ultrasonic Power	0.011	1	0.011	3.11	0.0932**	0.85
D-Coolant Pressure	0.017	1	0.017	4.76	0.0412*	1.31
Feed Rate $\times$ Spindle Speed	0.034	1	0.034	9.43	0.0060*	2.62
Feed Rate <sup>2</sup>	0.031	1	0.031	8.60	0.0082*	2.38
Spindle Speed <sup>2</sup>	0.061	1	0.061	16.67	0.0006*	4.69
Ultrasonic Power <sup>2</sup>	0.029	1	0.029	8.10	0.0100*	2.23
Coolant Pressure <sup>2</sup>	0.014	1	0.014	3.83	0.0646**	1.08
Residual	0.073	20	0.00364			
Lack of Fit	0.059	15	0.00391	1.37	0.3866**	
Pure Error	0.014	5	0.00284			1.08
Cor. Total	1.30	29				
Standard Deviation	0.060		R-Squared	0.9442		
Mean	0.74		Adjusted R <sup>2</sup>	0.9191		
Coefficient of Variation	8.14 %		Predicted R <sup>2</sup>	0.8205		
PRESS	0.023		Adequate Precision	24.042		

\*Significant. \*\*Not Significant

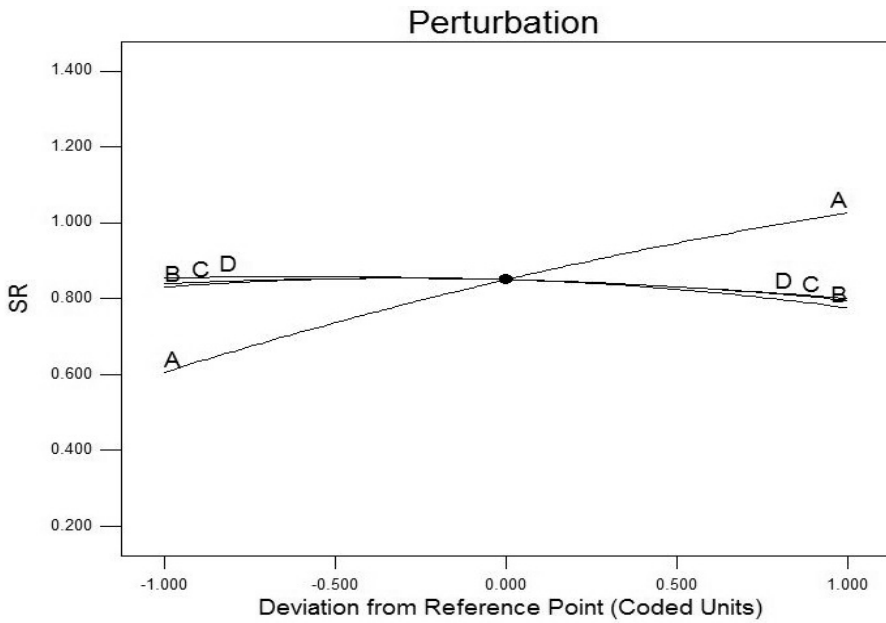


Figure 7. Perturbation plot for surface roughness.

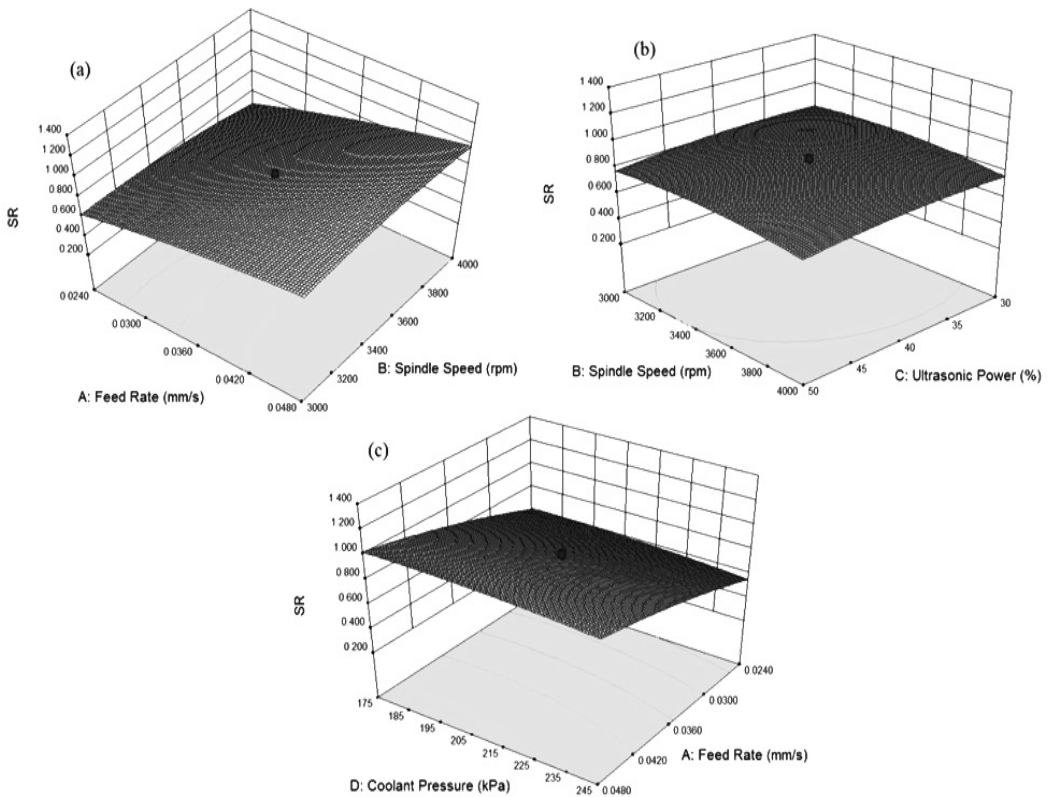


Figure 8. (a), (b), and (c) Two variables interactive effects of ultrasonic power, feed rate, coolant pressure, and spindle speed on SR.

### *Influences of investigated process variables on 'CT'*

The variables feed rate (A), spindle speed (B), ultrasonic power (C), interactive impacts of feed rate and spindle speed (A×B), second order term of feed rate (A<sup>2</sup>), spindle speed (B<sup>2</sup>), ultrasonic power (C<sup>2</sup>), and coolant pressure (D<sup>2</sup>) are observed to have significant effects on chipping thickness (CT) in RUM of alumina ceramic. The process variables, that is, feed rate (A) and spindle rotational speed (B), are revealed to contribute about 62% of the overall discrepancy in the response data. All these linear, interaction effect and second order terms of input process parameters possessing main contribution for CT are well detailed in Table 7.

Chipping thickness (CT) is found to be increased steeply, that is, 0.192 mm to 0.972 mm, as feed level incremented from 0.012 mm/s to 0.060 mm/s. The observed enhancement rate in CT with feed rate is higher than the decrement rate in CT found with other parameters, as shown in the perturbation graph for CT in Figure 9.

In the RUM of hard and brittle material such as alumina ceramic, edge chipping is likely to occur on the drilled hole as well as on the machined rod. The literature review on RUM of different ceramic materials reveals that the cutting force is developed during the process as the most influential factor that causes the edge chipping to occur (Jiao et al., 2005; Li et al., 2006). The higher the generated cutting force is during the machining, the larger the thickness of edge chipping will be. The stress distribution of the contact region amid the surface of work and tool can also expose out the mechanism of the chipping formation. This distribution of stress ( $\sigma$ ) can be computed as

$$\sigma = \frac{\text{Force}}{(\pi/4) \times (D_o^2 - D_i^2)} \quad (5)$$

The above equation further makes it confirm that the cutting force has more influence on the chipping thickness. The combined effects of input process parameters on CT are well illustrated with three-dimensional surface plots, as exemplified in Figure 10. The combined influence of feed rate and spindle speed on CT is represented in Figure 10(a). Higher chipping thickness is revealed as the feed rate of diamond impregnated core drill tool incremented. The increase in feed rate causes incremented cutting force to develop, and hence increased CT has been observed. As the level of spindle speed is enhanced from 2500 rpm to 4500 rpm, the penetration depth of the diamond abrasives is reduced, but the length of contact incremented. This fact causes the cutting force to be reduced at higher spindle speed. Therefore, reduction in chipping thickness (0.810 mm to 526 mm) has been observed as spindle speed increased (from 2500 rpm to 4500 rpm). Figure 10(b) depicts the 3D surface plot for spindle speed and ultrasonic power. Chipping thickness reduces from 0.670 mm to 0.583 mm as the ultrasonic power is enhanced from 20% to 60%. This can be associated with the fact that increased ultrasonic power develops reduced level of cutting force; hence, the chipping thickness decreased. These findings are well inconsistent with other studies performed on RUM of ceramics materials. Chipping thickness is found to be reduced at higher spindle speed. Figure 10(c) demonstrates the combined effects of feed rate and coolant pressure on CT. At higher pressure of coolant fluid, the swarf and chip dust can be effluent away from the machining zone more adroitly. Thus, the chances of tool jamming are reduced in addition to the cutting force. The higher the coolant fluid pressure is, the lower the cutting force produced

will be during machining. This fact further causes the reduction of chipping thickness over the machined rod. The interaction between feed rate and spindle speed is also found to produce an appreciable effect on chipping thickness.

**Table 6.** ANOVA results for chipping thickness.

Source	Sum of squares	dof	Mean square	F-value	p-value Prob> F	% Contribution
Model	1.20	10	0.12	39.02	< 0.0001*	
A-Feed Rate	0.62	1	0.62	201.51	< 0.0001*	49.60
B-Spindle Speed	0.15	1	0.15	49.28	< 0.0001*	12.00
C-Ultrasonic Power	0.031	1	0.031	10.08	0.0050*	2.48
D-Coolant Pressure	0.0047	1	0.0047	1.53	0.2308**	0.38
Feed Rate × Spindle Speed	0.016	1	0.016	5.27	0.0332*	1.28
Feed Rate × Coolant Pressure	0.0099	1	0.0099	3.25	0.0872**	0.79
Feed Rate <sup>2</sup>	0.13	1	0.13	41.49	< 0.0001*	10.40
Spindle Speed <sup>2</sup>	0.060	1	0.060	19.45	0.0003*	4.80
Ultrasonic Power <sup>2</sup>	0.089	1	0.089	29.06	< 0.0001*	7.12
Coolant Pressure <sup>2</sup>	0.23	1	0.23	73.88	< 0.0001*	18.40
Residual	0.058	19	0.0031			
Lack of Fit	0.041	14	0.0029	0.85	0.6336**	
Pure Error	0.017	5	0.00345			1.36
Cor Total	1.25	29				
Standard Deviation	0.055		R-Squared	0.9536		
Mean	0.62		Adjusted R <sup>2</sup>	0.9291		
Coefficient of Variation	8.98 %		Predicted R <sup>2</sup>	0.8563		
PRESS	0.18		Adequate Precision	20.195		

\*Significant. \*\*Not Significant

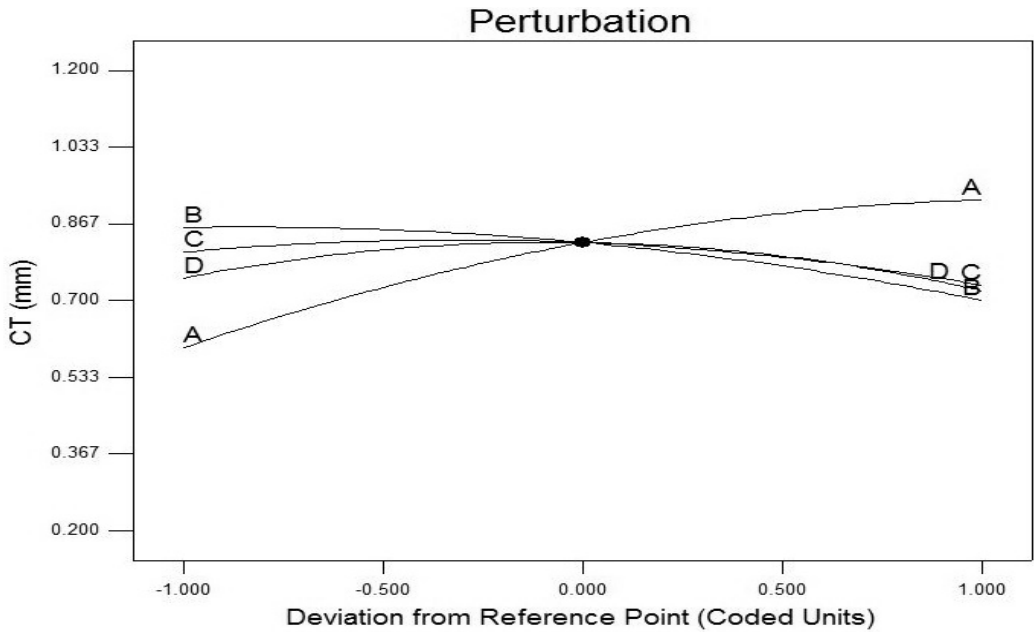


Figure 9. Perturbation plot for chipping thickness.

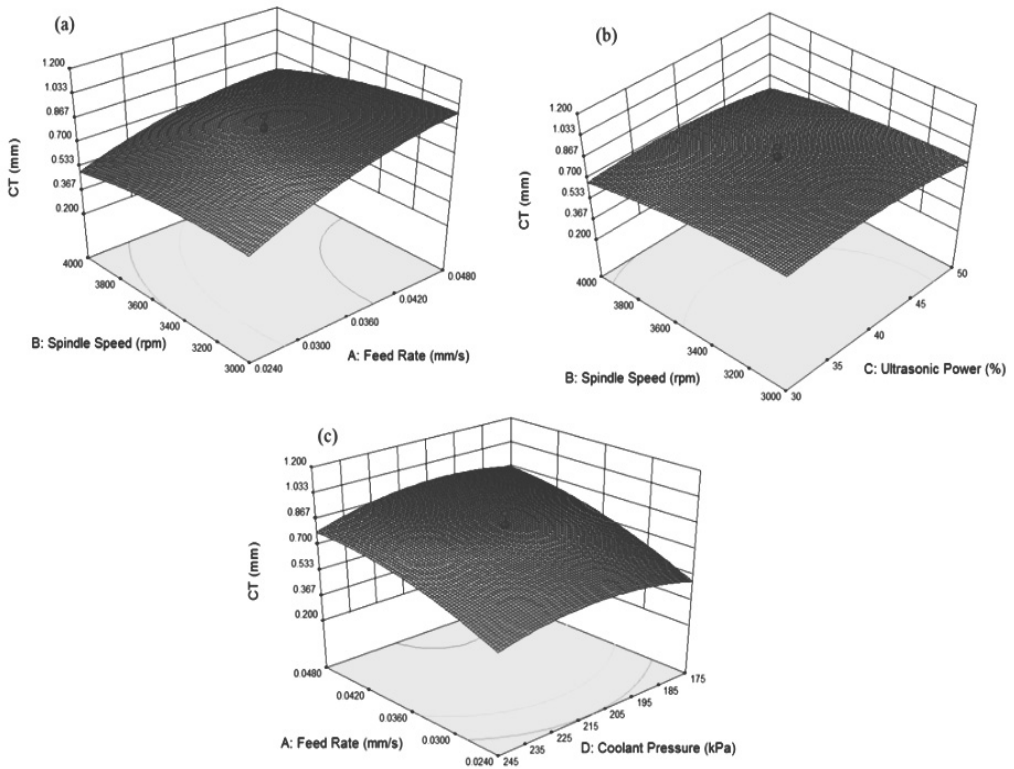


Figure 10. (a), (b), and (c) Two variables interactive effects of feed rate, spindle speed, ultrasonic power, and coolant pressure on chipping thickness.

### MICROSTRUCTURE ANALYSIS OF MACHINED SURFACE

The microstructure of the machined rod surface was observed using SEM analysis (EVO40, Carl Zeiss AG, Oberkochen, Germany). In rotary ultrasonic machining, the characteristics of the surface under process are primarily getting influenced by the consequence of feed rate, spindle speed, and ultrasonic power. Moreover, under few experimental conditions, apart from the brittle and plastic deformation of work material, the material removal can also take place as a combination of both failures. Therefore, for RUM of alumina ceramic material, the microstructure analysis has been endeavored with a view to check the applicability of the above disserted verities.

Before performing the SEM analysis, the workpiece samples (machined rods of alumina ceramic) are first carefully cleaned with the acetone solution and then coated with the layer of same conducting material (Au/Pd) by utilizing Sputter Coater Polaron (SC7640, Q.T. Limited, New-Haven, U.K.).

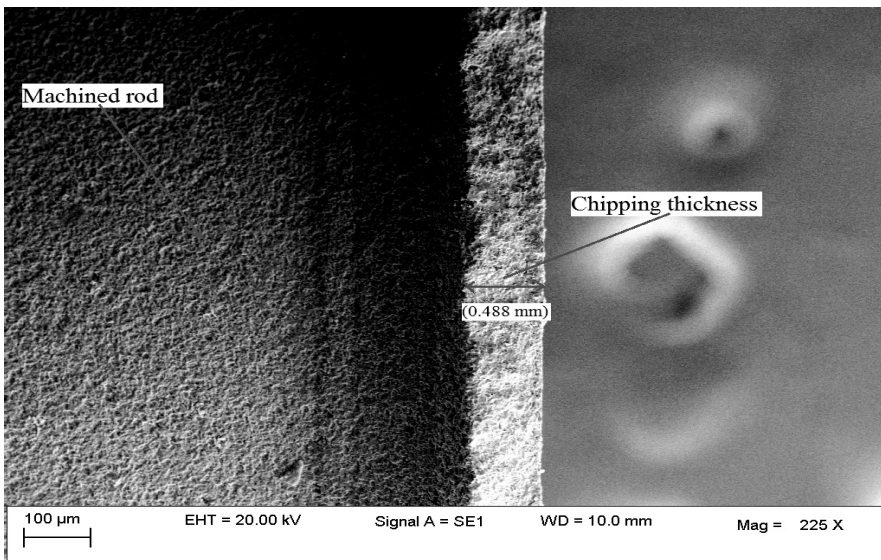


Figure 11. Illustration of chipping thickness observed for Exp. No. 1.

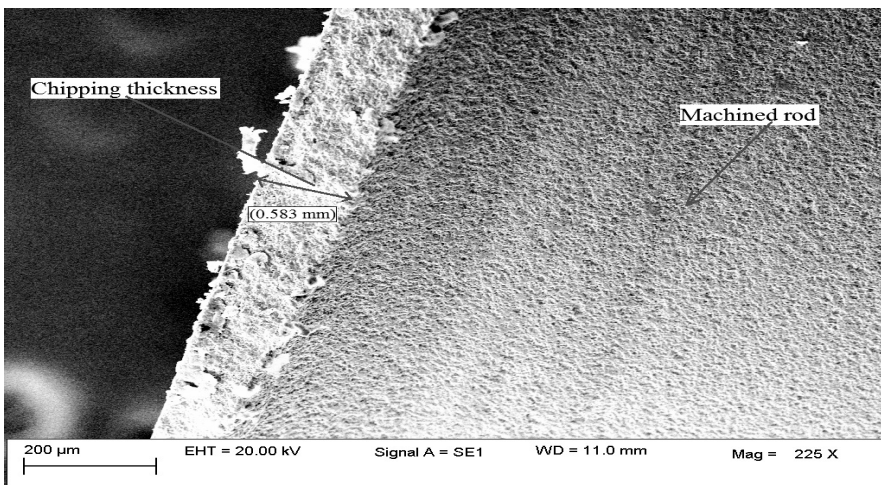
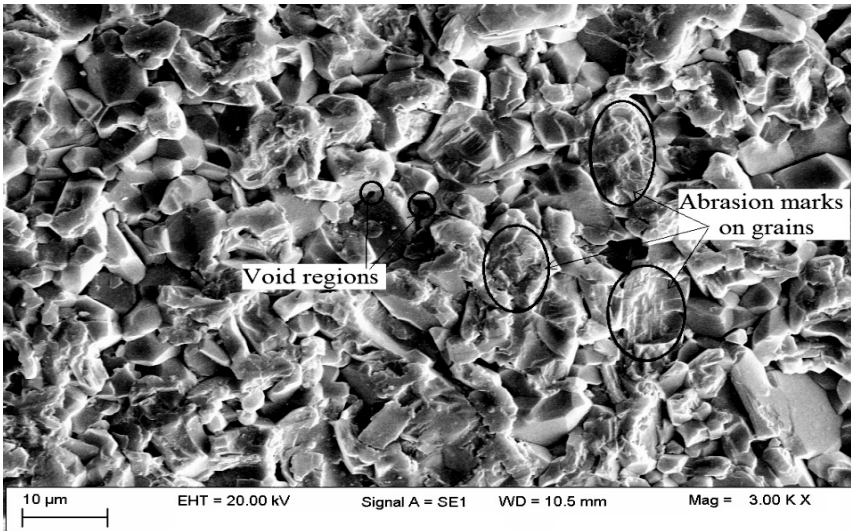
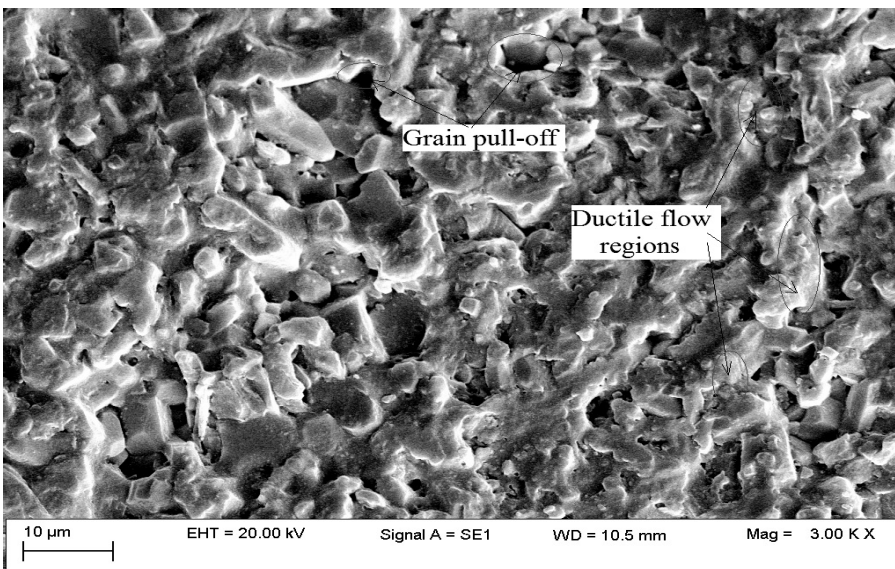


Figure 12. Illustration of chipping thickness observed for Exp. No. 22.



**Figure 13.** Microstructure of processed surface for Exp. No. 1.

For experiments no. 1 and 22, the chipping thickness can be noticeably revealed from the SEM micrograph of a machined rod at the magnification of 225 $\times$ , as shown in Figures 11 and 12, respectively. Figure 13 exemplifies the microstructure of machined rod surface processed under experimental conditions corresponding to experiment no. 1 at the magnification of 3000 $\times$ . The parametric setting for this experimental run was having a combination of moderate level of feed rate and spindle speed. In this SEM image, abrasion marks have been clearly observed on most of the alumina grains. The sharp edges present over the surface further promote the removal of material from work surface through brittle fracture, which can be attributed to the initiation and propagation of micro cracks.



**Figure 14.** SEM micrograph of machined surface for Exp. No. 17.

Figure 14 illustrates the microstructure of the machined surface corresponding to experiment no. 17 at the magnification of 3000 $\times$ . SEM image reveals the presence of mixed mode of material removal along with the dominant ductile mode failure of work material. It is also revealed that, at the lowest level of feed rate (0.012 mm/sec), the indentation depth of abrasives decrements, which further promotes the material to be removed in ductile mode after being pulverized. In RUM of alumina ceramic, crack propagation is often observed because the work surface under processing is getting stressed cyclically. In addition, material removal is in the form of bigger chunks, and the presence of sharp edge regions also favors the brittle failure of the work.

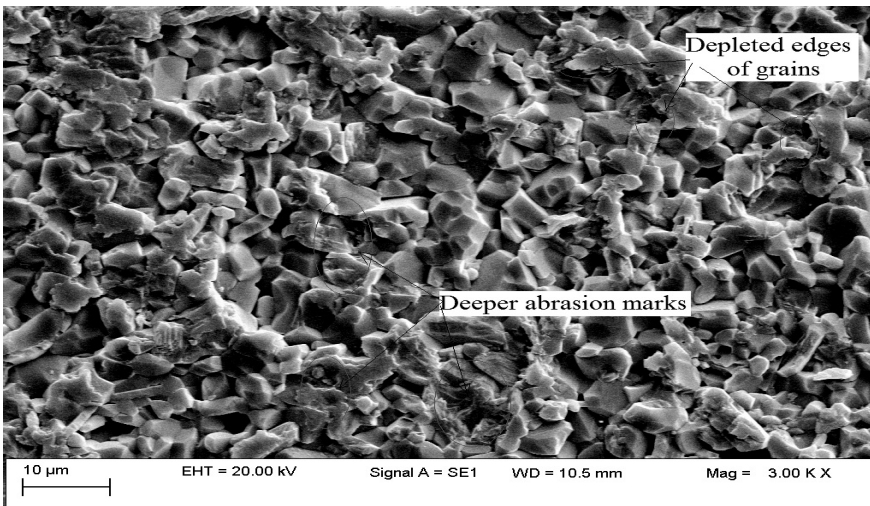


**Figure 15.** SEM micrograph of machined surface for Exp. No. 18.

Figure 15 demonstrates the microstructure of processed surface corresponding to experiment no. 18 at the magnification of 3000 $\times$ . This surface microstructure reveals the presence of highly dominant brittle mode deformation of the work material. At a higher level of feed rate (0.060 mm/sec), the depth of penetration of abrasives into the work surface incremented considerably, hence resulting in the presence of deeper abrasion marks, which further cause the material to be removed. In addition to this, the number of grains has been also observed possessing depleted edges. Furthermore, the instigation and promulgation of inter-granular and trans-granular cracks also cause the material removal in the form of larger chunks, which also favor the brittle failure of the workpiece.

### **OPTIMIZATION OF INPUT PROCESS VARIABLES FOR ‘SR (Ra)’ and ‘CT’**

After analyzing the experimental results, the investigated input process variables have also been optimized for considered process outcomes (i.e., SR and CT). This optimization work has been conducted using “desirability approach.”

In 1980, Derringer and Suich have prescribed desirability approach to optimize objectives (Singh et al., 2014).

### Single response optimization

The optimization of single response has been performed with a view to determine the optimum parametric setting of input factors, which can provide the most favorable results for the considered response. For the process variables to be optimized, the goals and range are illustrated in Table 7. The goal is set to “in range” for all the process variables, which means that parameters will be optimized through searching the space within the lower and upper limit. As per the desired situation, for both SR and CT, the goal is set ‘to minimize.’ All the variables are assigned equal weights and the same level of importance. The machining solution possesses an overall desirability value of ‘one’ or ‘closer to one’ selected as optimized solution. The optimized settings of process variables after being rounded up are detailed in Table 8. For the single response optimization, the optimized parametric condition for SR is as follows; feed rate 0.019 mm/s, spindle speed 4000 rpm, ultrasonic power 55%, and coolant fluid pressure 280 kPa. For CT, the optimized parametric setting is as follows: feed rate 0.017 mm/s, spindle speed 4500 rpm, ultrasonic power 50%, and coolant fluid pressure 245 kPa. At these optimum conditions, the confirmatory experimental runs have been conducted with two replications, and the predicted values and average of confirmatory experimental results for SR and CT are also tabulated in Table 8.

**Table 7.** Range of input variables for SR (Ra) and CT.

Variables	Goal	Lower limit	Upper limit	Weight	Importance
A: Feed Rate (mm/s)	in range	0.012	0.060	1	3
B: Spindle Speed (rpm)	in range	2500	4500	1	3
C: Ultrasonic Power (%)	in range	20	60	1	3
D: Coolant Pressure (kPa)	in range	140	280	1	3
SR ( $\mu\text{m}$ )	To minimize	0.289	1.241	1	3
CT (mm)	To minimize	0.192	0.972	1	3

**Table 8.** Experimental results for SR (Ra) and CT at optimized setting and confirmatory results.

S. No.	Response(s)	Optimized condition				Predicted values	Confirmatory results	Best experimental results
		A (mm/s)	B (rpm)	C (%)	D (kPa)			
1.	SR ( $\mu\text{m}$ )	0.019	4000	55	280	0.128	0.134	0.289
	CT (mm)	0.017	4500	50	245	0.070	0.073	0.192

The confirmatory results for SR and CT have been found to vary from the predicted values with the variation of 4.68% and 4.28%, respectively. The confirmatory experiments have also been analyzed and found within the 95% confidence interval. Table 9 depicts the point predictions at optimized parametric conditions for SR and CT.

Table 9. Point prediction at optimized parametric condition for SR (Ra) and CT.

Response	Predicted value	Confirmatory experimental results	95% CI low	95% CI high	95% PI low	95% PI high
For response:						
SR	0.128	0.134	0.005	0.251	-0.185	0.441
CT	0.070	0.073	-0.069	0.209	-0.247	0.387

### CONCLUSIONS

An experimental study has been performed to underscore the influence of input factors on SR (Ra) and CT in RUM of alumina ceramic. The following inferences can be made from the present investigation:

- Tool feed rate has been revealed as the most influential variable for both considered responses. The lowest CT was attained at a combination of high spindle speed and low level of feed rate. Lower feed rate resulted in the decrement in the penetration depth of diamond abrasives. Incremented spindle speed level also promotes the chances of material removal in ductile mode, which further produces the finer machined surfaces.
- Spindle speed at advanced level with smaller feed rate offers the most complimentary results in terms of CT, because, with this combination, the stress generated at the contact region between the tool and workpiece decreases. Higher spindle speed causes the decrement in the penetration depth and hence reduced cutting force generated, which further caused smaller CT. The parametric combination of lower feed rate and higher level of ultrasonic power, spindle speed, and coolant pressure was reported to be the most constructive solution for chipping thickness.
- The optimized parametric setting for SR was devised as follows: feed rate 0.019 mm/s, spindle speed 4000 rpm, ultrasonic power 55%, and coolant fluid pressure 280 kPa. The best parametric setting for CT was obtained as follows: feed rate 0.017 mm/s, spindle speed 4500 rpm, ultrasonic power 50%, and coolant fluid pressure 245 kPa.
- As the penetration depth of abrasives increases, the proportion of the brittle mode deformation has been revealed to be increased. This was happening because, at the larger depth of indentation, the material removal starts in the form of larger chunks and developed inter-granular cracks, further causing the grains to pull out. In RUM of alumina ceramic, crack propagation is often observed since the work surface under processing is getting stressed cyclically.

## REFERENCES

- Bertsche, E., Ehmann, K. & Malukhin, K. 2013.** Ultrasonic slot machining of a silicon carbide matrix composite. *International Journal of Advanced Manufacturing Technology* **66**(5-8): 1119-1134.
- Churi, N.J., Pei, Z.J., Shorter, D.C. & Treadwell, C. 2009.** Rotary ultrasonic machining of dental ceramics. *International Journal of Machining and Machinability of Materials* **6**(3-4): 270-284.
- Cong, W.L., Pei, Z.J. & Treadwell, C. 2014.** Preliminary study on rotary ultrasonic machining of CFRP/Ti stacks. *Ultrasonics* **54**(6): 1594-1602.
- Cong, W.L., Pei, Z.J., Feng, Q., Deines, T.W. & Treadwell, C. 2012.** Rotary ultrasonic machining of CFRP: a comparison with twist drilling. *Journal of Reinforced Plastics and Composites* **31**(5): 313-321.
- Dubey, A.K. & Yadava, V. 2008.** Laser beam machining- a review. *International Journal of Machine Tools and Manufacture* **48**: 609-628.
- Falamaki, C. & Beyhaghi, M. 2009.** Slip casting process for the manufacture of tubular alumina microfiltration membranes. *Materials Science-Poland* **27**(2): 427-441.
- Geng, D., Zhang, D., Xu, Y., He, F. & Liu, F. 2014.** Comparison of drill wear mechanism between rotary ultrasonic elliptical machining and conventional drilling of CFRP. *Journal of Reinforced Plastics and Composites* **33**(9): 797-809.
- Gong, H., Fang, F.Z. & Hu, X.T. 2010.** Kinematic view of tool life in rotary ultrasonic side milling of hard and brittle materials. *International Journal of Machine Tools and Manufacture* **50**: 303-307.
- Hu, P., Zhang, J.M., Pei, Z.J. & Treadwell, C. 2002.** Modeling of material removal rate in rotary ultrasonic machining: designed experiments. *Journal of Materials Processing Technology* **129**(1): 339-344.
- Jiao, Y., Liu, W.J., Pei, Z.J., Xin, X.J. & Treadwell, C. 2005.** Study on edge chipping in rotary ultrasonic machining of ceramics: an integration of designed experiments and finite element method analysis. *Journal of Manufacturing Science and Engineering* **127**(4): 752-758.
- Kataria, R., Kumar, J. & Pabla, B.S. 2015.** Experimental investigation into the hole quality in ultrasonic machining of WC-Co composite. *Materials and Manufacturing Processes* **30**(7): 921-933.
- Kataria, R., Kumar, J. & Pabla, B.S. 2016a.** Experimental investigation and optimization of machining characteristics in ultrasonic machining of WC-Co composite using GRA method. *Materials and Manufacturing Processes* **31**(5): 685-693.
- Kataria, R., Singh, R.P. & Kumar, J. 2016b.** An experimental study on ultrasonic machining of tungsten carbide cobalt composite materials. *AIMS Material Science* **3**(4): 1391-1409.
- Li, Z.C., Cai, L.W., Pei, Z.J. & Treadwell, C. 2006.** Edge-chipping reduction in rotary ultrasonic machining of ceramics: finite element analysis and experimental verification. *International Journal of Machine Tools and Manufacture* **46**(12): 1469-1477.
- Li, Z.C., Jiao, Y., Deines, T.W., Pei, Z.J. & Treadwell, C. 2005.** Rotary ultrasonic machining of ceramic matrix composites: feasibility study and designed experiments. *International Journal of Machine Tools and Manufacture* **45**(12): 1402-1411.
- Liu, J.W., Baek, D.K. & Ko, T.J. 2014.** Chipping minimization in drilling ceramic materials with rotary ultrasonic machining. *International Journal of Advanced Manufacturing Technology* **72**(9-12): 1527-1535.
- Patel, K.M., Pandey, P.M. & Rao, P.V. 2011.** Study on machinability of Al<sub>2</sub>O<sub>3</sub> ceramic composite in EDM using response surface methodology. *Journal of Engineering Materials and Technology* **133**: 021004-1-10.

- Pei, Z.J., Ferreira, P.M. & Haselkorn, M. 1995.** Plastic flow in rotary ultrasonic machining of ceramics. *Journal of Materials Processing Technology* **48**(1): 771-777.
- Singh, B., Kumar, J. & Kumar, S. 2014.** Experimental investigation on surface characteristics in powder-mixed electrodischarge machining of AA6061/10% SiC composite. *Materials and Manufacturing Processes* **29**(3): 287-297.
- Singh, R.P. & Singhal, S. 2016a.** Rotary ultrasonic machining: a review. *Materials and Manufacturing Processes* **31**(14): 1795-1824.
- Singh, R.P. & Singhal, S. 2016b.** An experimental study on rotary ultrasonic machining of macor ceramic. *Journal of Engineering Manufacture* doi: 10.1177/0954405416666897.
- Singh, R.P. & Singhal, S. 2016c.** Experimental study on rotary ultrasonic machining of alumina ceramic: microstructure analysis and multi-response optimization. *Journal of Materials: Design and Applications* doi: 10.1177/1464420716657370.
- Singh, R.P. & Singhal, S. 2016d.** Experimental investigation of machining characteristics in rotary ultrasonic machining of quartz ceramic. *Journal of Materials: Design and Applications* doi: 10.1177/1464420716653422.
- Singh, R.P. & Singhal, S. 2017a.** Investigation of machining characteristics in rotary ultrasonic machining of alumina ceramic. *Materials and Manufacturing Processes* **32**(3): 309-326.
- Singh, R.P. & Singhal, S. 2017b.** Rotary ultrasonic machining of macor ceramic: An experimental investigation and microstructure analysis. *Materials and Manufacturing Processes* **32**(9): 927-939.
- Singh, R.P., Kumar, J., Kataria, R. & Singhal, S. 2015.** Investigation of the machinability of commercially pure titanium in ultrasonic machining using graph theory and matrix method. *Journal of Engineering Research* **3**(4): 75-94.
- Ya, G., Qin, H.W., Xu, Y.W. & Zhang, Y.S. 2001.** An experimental investigation on rotary ultrasonic machining. *Key engineering materials* **202**: 277-280.
- Zeng, W.M., Xu, X.P. & Pei, Z.J. 2009.** Experimental investigation of tool wear in rotary ultrasonic machining of alumina. *Key Engineering Materials* **416**: 182-186.
- Zhang, C., Cong, W., Feng, P. & Pei, Z. 2014.** Rotary ultrasonic machining of optical K9 glass using compressed air as coolant: A feasibility study. *Journal of Engineering Manufacture* **228**(4): 504-514.
- Zhang, C.L., Feng, P.F., Wu, Z.J. & Yu, D.W. 2011.** An experimental study on processing performance of rotary ultrasonic drilling of K9 glass. *Advanced Materials Research* **230**: 221-225.

*Submitted:* 26/04/2016

*Revised* : 19/03/2017

*Accepted* : 21/03/2017